Optics Letters

Drying-mediated optical assembly of silica spheres in a symmetrical metallic waveguide structure

Tian Xu,[1] Cheng Yin,[2,3,*] XueFen Kan,[3] TingChao He,[4] Qingbang Han,[3] Zhuangqi Cao,[2] and Xianfeng Chen[2]

[1]Physics Department, Nantong University, No. 9, Seyuan Road, Nantong, Jiangsu 226007, China
[2]The State Key Laboratory on Fiber Optic Local Area Communication Networks and Advanced Optical Communication Systems, Department of Physics and Astronomy, Shanghai JiaoTong University, Shanghai 200240, China
[3]Jiangsu Key Laboratory of Power Transmission and Distribution Equipment Technology, Hohai University, Changzhou 213022, China
[4]College of Physics and Energy, Shenzhen University, Shenzhen 518060, China
*Corresponding author: cyin.phys@gmail.com

Received 12 May 2017; accepted 29 June 2017; posted 3 July 2017 (Doc. ID 295824); published 25 July 2017

We describe the optical trapping application of a simple metallic slab optical waveguide structure, and demonstrate the influence of the excited guided modes on the aggregation behavior of silica particles during the irreversible evaporation process. Periodic horizontal stripes are formed by the highly ordered assemblies of the silica spheres, which is explained via the interference effect between the forward propagating modes and its reflection at the solvent surface. Particularly, several layers consisting of high-density particles are discernible in the stripe zones due to the optical binding, while no particles locate between these stripes. Completely different from the self-assembly patterns in the evaporating solvent without excitation of optical modes, this Letter demonstrates the versatility in the possible patterns of the optical assembly by a coupling waveguide with more complex structures.

OCIS codes: (230.7390) Waveguides, planar; (310.2785) Guided wave applications; (140.7010) Laser trapping.

https://doi.org/10.1364/OL.42.002960

Optical tweezers are powerful non-contact tools to trap, move, and rotate small objects in a liquid environment, where a gradient force directed towards the focus is exerted on the trapped particles by a strongly converging laser [1–3]. Their widespread applications in biology [4,5] and physical sciences have led to a burst of investigations to craft multifunctional optical trapping system. For example, the ability of the plasmonic nanostructure to concentrate light well beyond the diffraction limit has been applied to produce nano-optical tweezers for the nanometer-sized particles [6]. Holographic optical tweezers (HOT) are a widely researched technology to create various dynamical optical traps in arbitrary three-dimensional configurations via computer designed holograms [4,7]. In order to achieve higher diversity in the possible optical organization of particles, much effort has been devoted to realizing more complicated optical landscapes than those of a simple focused laser beam. For instance, the family of Ince–Gaussian beams was used to create complex two-dimensional optical traps for multiple particles [8]. For another illustration, Ag nanoparticles are selectively assembled into doughnut-like patterns under the irradiation of the doughnut beams [9]. The surface plasmon-induced evanescent fields at a patterned metallic interface were also applied to operate small polystyrene microbeads. Its force field can be accurately controlled by adjusting incident parameters such as incident angle and polarization to realize ultra-gentle manipulation of the trapped objects [10].

Instead of using strongly focused beams, guided modes excited in a very simple metallic planar waveguide structure were adopted in this Letter to trap colloidal particles. Furthermore, ordered assemblies of the trapped particles were observed to form patterned arrays when the solvent evaporation is completed. To the best of our knowledge, experimental evidence for optical trapping via guided modes in planar waveguide has remained scare. On the contrary, waveguide structure can provide not only efficient amplification to overcome Brownian random forces due to its high quality confinement of the radiation, but also enable continuous and accurate adjustment of the optical landscape via tuning incident parameters, including wavelength, polarization, and incident angle. This Letter also provides a concrete example of how the drying mediated self-assembly of colloidal particles [11] varies in the presence of the light-induced force (LIF) field. The simultaneous trapping of several hundred particles with negligible interaction is not an optical matter, which only refers to the close packing assemblies due to optical binding [12] with a structure akin to crystals. Grzegorczyk *et al.* demonstrated a laser-trapped optical mirror by assembling a monolayer of optically bound particles at a dielectric surface in water [13]. The optical binding effect can be described as a first trapped particle focus parts of light, while a second particle is trapped closely by this focus.

In our experiment, closely packed particles pile up in several layers with a crystal-like organization, which can be attributed to this effect. Since the excited guided modes propagate along the waveguide far beyond the incident spot, it may be a potential candidate to produce large-scale optical matter, which remains challenging [14]. Generally speaking, in this Letter, a regular pattern formed by closely packed silica beads was optically assembled via the excitation of the guided modes in a metallic slab waveguide structure, which is explained by the interference of the guided mode.

The waveguide structure and the light path we adopted are plotted in Fig. 1(a), where a sample cell of 0.7 mm thick is sandwiched between a 0.3 mm thick upper glass slab and a 200 nm thick Ag substrate. Another thin Ag film about 30 nm is deposited on the upper glass slab to act as the coupling layer. When the sample cell is filled with silica beads colloid, the guiding layer of 1 mm thick consists of two layers, i.e., the colloid layer and the upper glass slab. The waves propagate along the z-direction of a Cartesian coordinate system, and the x-axis is perpendicular to the waveguide surface. We refer to this structure as symmetrical metal cladding waveguide (SMCW), which enables directing coupling from the free space [15].

When the incident angle fulfills the phase-match condition, i.e., the component of the wave vector in the z-axis direction equals the propagation constant β, energy is coupled into the waveguide, and the excited oscillating guided mode of high mode order ($>10^3$) propagates along the guiding layer [16]. The propagation constant β for the guided modes can be obtained by solving the dispersion equation of the SMCW chip [17]. In the x direction, a standing wave pattern is expected in the guiding layer due to the metallic reflection, which provides the gradient forces for the optical trapping. Note that the SMCW is polarization independent [18], and the particles used are isotropy, so we are not concerned about the polarization characteristics in this Letter. The light source is a 100 mW laser of 785 nm emitted from a single longitudinal mode laser (TE-polarized, LBX-785S-100-CIR-PP, Oxxius Co., France). Two apertures with a diameter of 1 mm are placed with distances about 0.5 m to further confine the divergence of the incident beam. A series of resonance dips appear in the measured reflection spectrum, as shown in Fig. 2, and each dip corresponds to a specific guided mode. Since the exact number of the mode order is not important in our experiment, any dip can be used to couple the energy into the guiding layer. The term "mode density" is used to refer to the number of modes per incident angle, so large mode density facilitates the experimental operation.

In our experiment, 0.05 g silica spheres are dissolved in 50 ml of absolute ethanol and ultra-sonicated at 100 W for 3 h. Figure 1(c) shows that the silica spheres are nearly spherical and have an average diameter of 260 nm. The colloid is then injected into the sample cell of the SMCW chip, which is placed vertically. It is important that the guiding layer is of millimeter thick, so the mode density is extremely high. Through monitoring the reflectivity, a specific guided mode can be excited by slightly adjusting the incident angle θ. Then we leave the experimental setup untouched until all the ethanol is evaporated. Most of the silica spheres are deposited on the bottom of the sample cell. Afterward, the laser is turned off, and the waveguide chip is left for 6 h, as the room temperature is fixed at 25 deg by an air condition. Then we remove the upper glass slab carefully, and the side coated with Ag coupling film is always kept down. Figure 3 shows SEM image of the guided mode assembled morphologies of the trapped silica beads on the inner side of the upper glass slab.

For comparison, Fig. 4 shows the self-assembled morphologies resulting from the homogeneous evaporation without the excitation of the guided modes. In Fig. 4(a), the waveguide chip is placed in the same way as that of Fig. 3. In Fig. 4(b), the waveguide chip is horizontally placed with the Ag coupling layer located in the bottom, so the gravity force is in the negative z direction. Comparing Figs. 3 and 4, it is clear that although the laser beam has not been focused by an objective lens in our experiments, the simple SMCW structure provides sufficient confinement of the radiation to alter the assembled morphologies of the mesoscopic particles.

Several remarks can be made on the above results. First, instead of the vertical patterns parallel to the gravity direction in Fig. 4(a), only horizontal stripes can be discerned when the

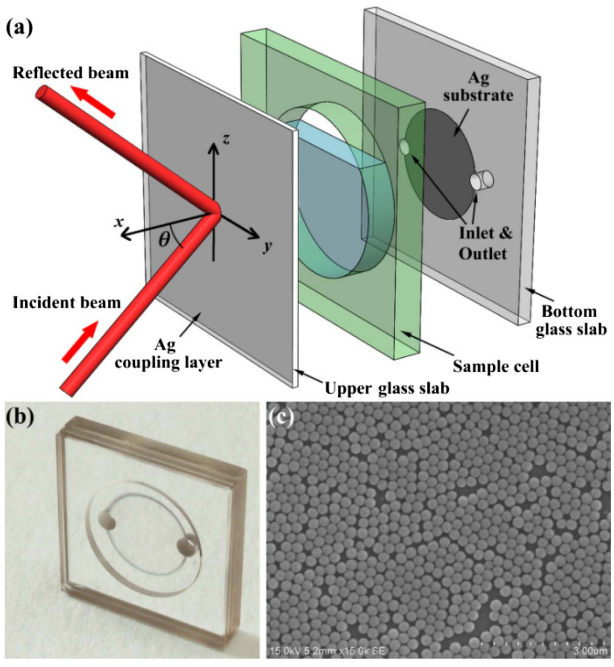

Fig. 1. (a) Schematic diagram of the SMCW chip and guided mode excitation via free space coupling, (b) photo of the sample cell before the deposition of the Ag coupling films, and (c) SEM of the silica spheres whose diameter is roughly 260 nm.

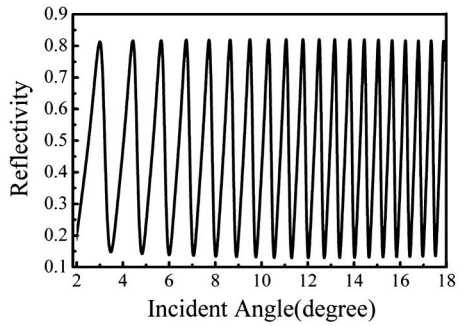

Fig. 2. Experimental measured reflection spectrum of an empty SMCW chip via a homemade $\theta/2\theta$ goniometer.

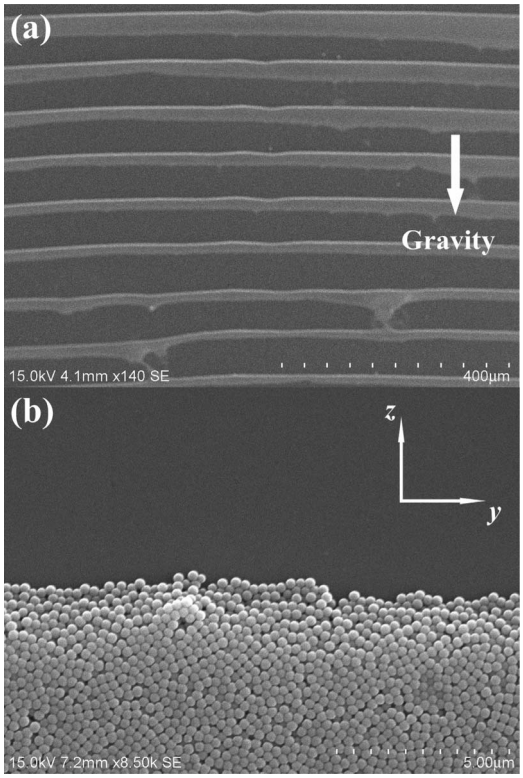

Fig. 3. Assembly of silica spheres on the inner surface of the upper glass slab. (a) Packing assemblies of particles form horizontal stripes, while very few particles can be found between two adjacent particle stripes. The white arrow denotes the gravity direction. (b) Density of the deposited particles in the stripe zone is so high that several layers can be discerned, and the Cartesian coordinate system is in consistent with the one used in Fig. 1.

guided mode interacts with the colloids. What is more interesting is that the particles of very high density are piled up in the "stripe zones," while very few particles are found between. Figure 3(b) clearly shows that several layers consisting of closely packed particles can be distinguished, which is not found in the comparing experiments. Since all the particles are deposited onto the upper glass slab eventually, the average particle density of Fig. 4(b) is much higher than that of the other experiments, i.e., Figs. 3 and 4(a). Please note that Fig. 1(c) is a close view of Fig. 4(b), which reveals that only a single layer of particles is observable, and no close packing phenomenon occurs in Fig. 1(c). We suggest that the optical binding effect is responsible for the crystal-like organization in Fig. 3(b). Finally, it needs to be pointed out that the patterned region in Fig. 3 is much larger than the beam spot on the waveguide surface of the incident beam. To understand these characteristics of the optical assembly, we performed electrodynamics simulations of a simplified SMCW model using a transfer matrix method and a finite element method (COMSOL multiphysics).

It is difficult to model the actual SMCW chip of millimeter scale that we used in the experiment due to the size issue. Thus, a simple SMCW model consisting of only three layers is adopted, and the homogeneous guiding layer is only 4.5 μm thick. Figure 5 plots the reflection spectrum calculated by a transfer matrix method, and the incidence is TE-polarized.

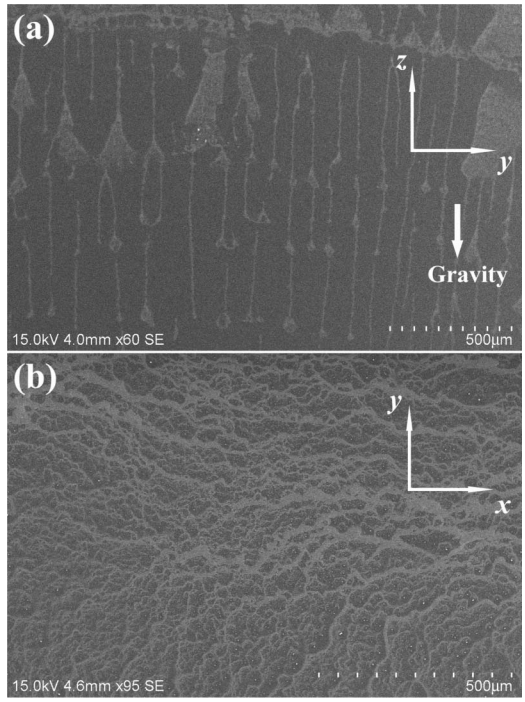

Fig. 4. Comparison of experimental results with the silica sphere solution of the same density. (a) SMCW chip stands vertically without the excitation of the guided modes. The white arrow denotes the gravity direction. (b) SMCW chip is positioned horizontally, and no laser source is involved.

The parameters are a coupling layer thickness $d_{\text{couple}} = 30$ nm, the substrate thickness $d_{\text{sub}} = 200$ nm, and the dielectric constant of silver is $\varepsilon_{\text{Ag}} = -16.5 + 1.06i$ for the incident wavelength $\lambda = 700$ nm, $\varepsilon_{\text{Air}} = 1$ for air, and $\varepsilon_{\text{Water}} = 1.69$ for water. A transition boundary condition is applied to simulate the coupling silver film. As can be seen from Fig. 5, the finite element simulations fit well with the

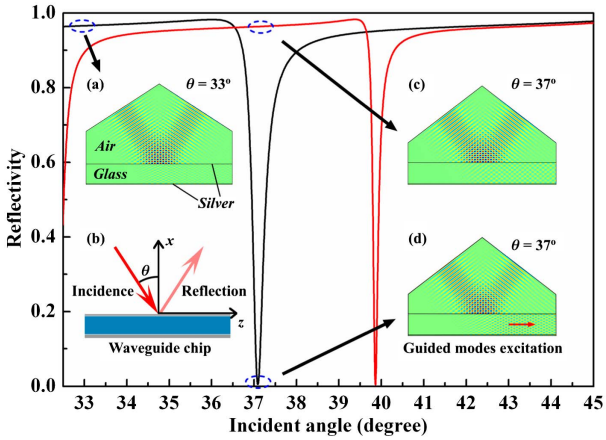

Fig. 5. Calculated reflection spectrum of a simplified three-layer model for water (black) and air (red). (a) Normalized y component of the electric field E_y of the SMCW chip at a non-resonant angle. (b) Schematic diagram of the simplified three-layer model of the finite element analysis. (c), (d) Normalized E_y at the same incident angle for a non-resonant case (c, air) and resonant case (d, water).

results of the transfer matrix method that the guided mode can only be excited when the incident angle fulfills the phase-match condition. When the guided mode is excited, energy is transferred from the reflected beam into the guiding layer, and a resonant dip is formed in the reflection spectrum. For a non-resonant incident angle, most energy is reflected, and only a very small portion of energy is coupled into the waveguide, which is due to the Gaussian beam used in the finite element analysis. One should also note that only a rightward travelling guided mode is excited in Fig. 5(d).

In order to simulate the evaporation process in our experiments, we vary the model in Fig. 5(d) by dividing the guiding layer into two parts. As can be seen from the model in Fig. 6, the left part of the guiding layer is filled with water ($\varepsilon_{\mathrm{Water}} = 1.69$), and the right part contains air ($\varepsilon_{\mathrm{Air}} = 1$). As is clear from Fig. 5, a specific guided mode can be excited in the water region when the incident angle is fixed at 37 deg, while no energy can be coupled into the air region. We are most interested in the electric field intensity at the water-air interface, which is crucial for the particle-deposition probability on the inner wall of the sample cell.

The simulation results are presented in Fig. 6, where the water-air interface is shifted leftward continuously to represent the slow evaporation process of water in the sample cell. From (a) to (c), the shifts of the interface are very small, and the optical field intensity at the water-air interface is high, low, and high, respectively. Similar remarks can also be applied to (d)–(f). Several conclusions can be drawn from here. First, the propagating guided mode will be reflected at the water-air interface, which is obvious when we compare the left edges of the guiding layer in Figs. 5(d) and 6. Secondly, the reflected mode and the rightward travelling mode will interfere with each other. As the height of the water-air interface varies continuously, the phase difference between the two interfering modes also changes continuously. As a result, constructive interference and destructive interference occur alternately, which can be seen in Fig. 6. Among the six simulations, only (b) and (e) correspond to the case of destructive interference. In the case of constructive interference, the field intensity at the interface is much stronger than that of the excited guided mode in Fig. 5(d) while, in the case of destructive interference, the field intensity at the interface is even weaker than the intensity of the reflected mode at the left edge of the guiding layer. This may be used to explain why no particle can be found in the middle area of two stripe zones in our experiment. A possible explanation for the crystal-like organization in the stripe zone can be attributed to the combining effect of the optical binding and the high intensity of the constructive interference. Finally, as can be seen from Fig. 6, the interference patterns occupy a much larger region than the incident spot, since the excited guided mode propagates along the guiding layer. This is the reason why the observed horizontal pattern in Fig. 3 is much larger than the laser beam waist.

In summary, instead of using a strongly focused laser beam, the guided mode excited in a simple planar metallic optical waveguide structure, i.e., SMCW chip, is applied to trap silica beads of 260 nm in absolute ethanol. During the slow evaporation process of the solvent, horizontal stripe patterns consisting of closely packed particles are optically assembled, which is completely different from the self-assembled morphologies without the guided mode-particle interaction. The observed

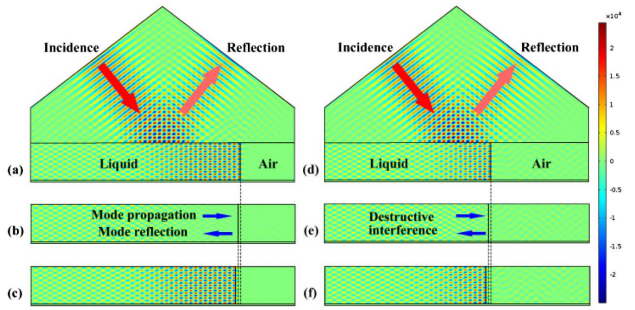

Fig. 6. Finite element analysis of the normalized E_y of the simplified model at resonance during the drying process. The incident angle is 37 deg.

phenomenon is fully explained through numerical simulation, that the interference intensity at the colloid-air interface is responsible for the horizontal stripe patterns. We suggest that optical binding is the reason for the close packing assemblies in the stripe zone, but further evidence is required to prove these strips are indeed optical matter. These demonstrated examples might excite further investigations and applications in the optical trapping and assembly issues via other waveguide structures, which feature higher diversity in the range of possible optical landscapes.

Funding. Natural Science Foundation of Jiangsu Province (BK20140246, BK20160417); National Natural Science Foundation of China (NSFC) (11404092, 11404219, 11574072, 61125503).

REFERENCES

1. D. G. Grier, Nature **424**, 810 (2003).
2. M. Padgett and R. Bowman, Nat. Photonics **5**, 343 (2011).
3. M. Dienerowitz, M. Mazilu, and K. Dholakia, J. Nanophoton. **2**, 021875 (2008).
4. G. R. Kirkham, E. Britchford, T. Upton, J. Ware, G. M. Gibson, Y. Devaud, M. Ehrbar, M. Padgett, S. Allen, L. D. Buttery, and K. Shakesheff, Sci. Rep. **5**, 8577 (2015).
5. M. Habaza, B. Gilboa, Y. Roichman, and N. T. Shaked, Opt. Lett. **40**, 1881 (2015).
6. M. L. Juan, M. Righini, and R. Quidant, Nat. Photonics **5**, 349 (2011).
7. E. R. Shanblatt and D. G. Grier, Opt. Express **19**, 5833 (2011).
8. M. Woerdemann, C. Alpmann, and C. Denz, Appl. Phys. Lett. **98**, 111101 (2011).
9. S. Lto, H. Yamauchi, M. Tamura, S. Hidaka, H. Hattori, T. Hamada, K. Nishida, S. Tokonami, T. Ltoh, H. Miyasaka, and T. Lida, Sci. Rep. **3**, 3047 (2013).
10. M. Righini, G. Volpe, C. Girard, D. Petrov, and R. Quidant, Phys. Rev. Lett. **100**, 186804 (2008).
11. E. Rabani, D. R. Reichman, P. L. Geissier, and L. E. Brus, Nature **426**, 271 (2003).
12. S. K. Mohanty, K. S. Mohanty, and M. W. Berns, Opt. Lett. **33**, 2155 (2008).
13. T. M. Grzegorczyk, J. Rohner, and J. M. Fournier, Phys. Rev. Lett. **112**, 023902 (2014).
14. Z. Yan, M. Sajjan, and N. F. Scherer, Phys. Rev. Lett. **114**, 143901 (2015).
15. C. Yin, Y. Lu, T. Xu, D. Z. Wei, Y. L. Jin, J. H. Fang, C. N. Wang, and M. Z. Huang, J. Raman Spectrosc. **47**, 560 (2016).
16. H. Lu, Z. Cao, H. Li, and Q. Shen, Appl. Phys. Lett. **85**, 4579 (2004).
17. C. Yin, J. Sun, X. Wang, C. Zhu, Q. Han, Z. Di, and Z. Cao, Europhys. Lett. **100**, 44001 (2012).
18. H. Li, Z. Cao, H. Lu, and Q. Shen, Appl. Phys. Lett. **83**, 2757 (2003).